

# CPAny: Couple With Any Encoder to Refer Multi-Object Tracking

Weize Li, Yunhao Du, Qixiang Yin, Zhicheng Zhao, Fei Su, Daqi Liu

**Abstract**—Referring Multi-Object Tracking (RMOT) aims to localize target trajectories specified by natural language expressions in videos. Existing RMOT methods mainly follow two paradigms, namely, one-stage strategies and two-stage ones. The former jointly trains tracking with referring but suffers from substantial computational overhead. Although the latter improves computational efficiency, its CLIP-inspired dual-tower architecture restricts compatibility with other visual/text backbones and is not future-proof. To overcome these limitations, we propose CPAny, a novel encoder-decoder framework for two-stage RMOT, which introduces two core components: (1) a Contextual Visual Semantic Abstractor (CVSA) performs context-aware aggregation on visual backbone features and projects them into a unified semantic space; (2) a Parallel Semantic Summarizer (PSS) decodes the visual and linguistic features at the semantic level in parallel and generates referring scores. By replacing the inherent feature alignment of encoders with a self-constructed unified semantic space, CPAny achieves flexible compatibility with arbitrary emerging visual / text encoders. Meanwhile, CPAny aggregates contextual information by encoding only once and processes multiple expressions in parallel, significantly reducing computational redundancy. Extensive experiments on the Refer-KITTI and Refer-KITTI-V2 datasets show that CPAny outperforms SOTA methods across diverse encoder combinations, with a particular 7.77% HOTA improvement on Refer-KITTI-V2. Code will be available soon.

## I. INTRODUCTION

In contrast to conventional cross-modal tasks (e.g., image-text matching / retrieval [1–3] or referring single-object tracking [4–6]), Referring Multi-Object Tracking (RMOT) [7] establishes dynamic correspondence between textual descriptions and spatiotemporal trajectories of one or multiple unique targets in video sequences. As illustrated in Fig. 1, RMOT extends traditional Multi-Object Tracking (MOT) by introducing a series of unique expressions. The tracker in RMOT is required not only to establish a correspondence between the expressions and the objects, but also to track these objects throughout the video. For instance, given an expression like “car on the left”, the model is required to provide the trajectories of all cars on the left side of the video while filtering out semantically irrelevant objects. Compared with MOT, RMOT places greater emphasis on generalization of classes. Meanwhile, in contrast to typical image-text matching, it also demands a more fine-grained understanding of local details.

Existing RMOT methods mainly follow two architectural paradigms: one-stage and two-stage. Current one-stage methods [7–9] usually augment the conventional MOT architecture MOTR [10] with auxiliary classification modules to verify

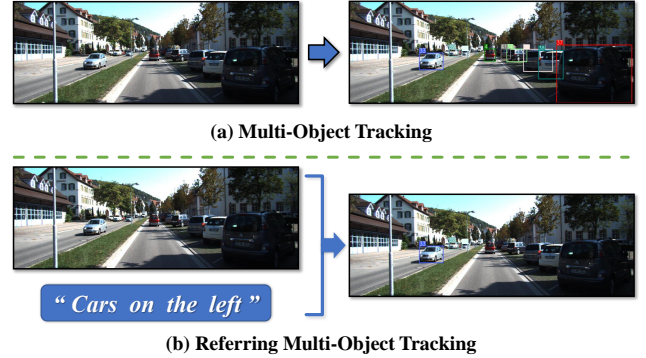


Fig. 1. Comparison between MOT and RMOT. Compared to MOT (a), which aims to track all targets for given classes, RMOT [7] (b) emphasizes a deeper understanding of the fine-grained attributes of targets (such as category, color, location, etc.) and the cross-modal interaction between these attributes and natural language.

expression-target correspondence, as visualized in Fig. 2 (a). Although one-stage methods enable end-to-end referring tracking, they still rely on original tracking annotations to learn the multi-object tracking capability of MOTR [10], thus having substantial computational overhead. In contrast, two-stage methods [11] adopt a decoupled strategy by developing specialized cross-modal matchers that operate on trajectory proposals generated by off-the-shelf trackers. This modular design inherently provides greater flexibility in tracker selection and scalability across diverse scenarios.

However, although representative two-stage methods like iKUN [11] achieve architectural decoupling from trackers, they still exhibit limitations in encoder flexibility. As shown in Fig. 2 (b), the two-stage methods inherit the dual-tower structure of CLIP [1] to leverage its modality alignment capability. This design inherently ties the framework to CLIP’s specific visual-textual encoding spaces, thereby restricting compatibility with other emerging backbones (e.g., Swin Transformers [12] or BERT-based [13] text encoders) and being constrained by CLIP’s upper limit. We further quantitatively verify the weak adaptability of iKUN [11] in the Supplementary Material. Compared to encoder pairs with modality alignment, where more focus is placed on specialized visual / text encoders, the architecture of current methods is fundamentally difficult to adapt to new advancements. Additionally, trained directly on image-text pairs, CLIP lacks sufficient explicit region-based modeling capabilities. To compensate, advanced two-stage methods [11] capture contextual features by performing repeated encoding of both global images and cropped target images. The spatial overlap between the cropped and the

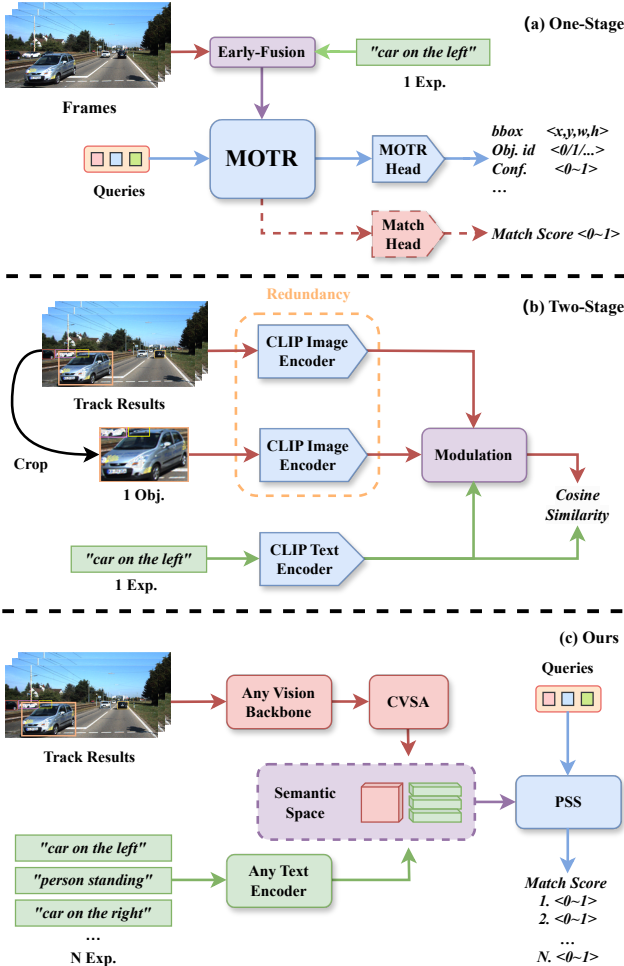


Fig. 2. The comparison among previous RMOT frameworks and ours. (a) shows the common one-stage methods. Based on MOTR, the one-stage methods perform early fusion and introduce an additional matching head. (b) illustrates two-stage methods, which utilize the CLIP visual-textual feature space and feed both global and cropped images into the image encoder to enhance the contextual information. (c) presents the proposed CPAny, which can be coupled with any visual backbone and any text encoder. After extracting visual semantics through the CVSA, the PSS decodes the matching results of the targets in the semantic space.

global images, along with the irrelevant background, causes great computational redundancy.

To address these limitations, we propose a novel encoder-decoder framework for two-stage RMOT, namely CPAny. As depicted in Fig. 2 (c), CPAny enables flexible integration with arbitrary visual/text encoders while incorporating a Contextual Visual Semantic Abstractor (CVSA) and a Parallel Semantic Summarizer (PSS), and eliminates the strong dependency on the inherent modality alignment of encoders, supporting seamless coupling with any visual backbone and any text encoder. Our contributions can be summarized as follows:

(1) We propose a novel future-proof encoder-decoder framework, namely CPAny, which eliminates dependency on inherent modality alignment via a self-constructed unified semantic space, thus enhancing adaptability to new advancements and flexibility.

(2) We introduce CVSA that distills trajectory-aware fea-

tures from global visual representations and projects them into a unified semantic space. It extracts contextual features through single-pass encoding in one forward propagation, reducing computational redundancy.

(3) A multi-modal decoder named PSS is constructed to fuse linguistic features with visual semantics to generate referring scores. Our novel parallel decoding strategy in PSS significantly accelerates inference speed in two-stage RMOT.

(4) CPAny surpasses current state-of-the-art (SOTA) methods in both performance and efficiency on widely used RMOT datasets, Refer-KITTI [7] and Refer-KITTI-V2 [8], across various combinations of visual / text encoders, demonstrating its superiority and robustness.

## II. RELATED WORK

### A. Referring Single Object Tracking

Referring Single Object Tracking (RSOT) has been studied for several years. Most SOTA methods [14–16] follow classic tracking strategies, integrating advancements in referring video segmentation [17] (or detection [18]) and focusing on end-to-end joint tracking algorithms. JointVLT [19] guides the model to perform grounding in the first frame by inputting only a zero-pad, and then continuously tracks the target in subsequent frames based on template and expression. TransVLT [20] uses a set of proxy tokens for cross-modal information fusion, which project linguistic features and generate kernel vectors to modulate visual features. Instead of directly decoding the bounding boxes, MMTrack [21] constructs a set of queries from expression and bounding box cues and generates the target trajectories using an autoregressive approach. Although RSOT has made significant achievements [22, 23], its development is limited by highly limited task scenarios.

### B. Referring Multi Object Tracking

TransRMOT [7] has pioneered RMOT by introducing the Refer-KITTI dataset and a baseline model based on MOTR [10]. In RMOT, expressions can refer to multiple objects, a single object, or even lose reference to the target. Building on TransRMOT [7], MLS-Track [9] further designs a multi-level semantic interaction module to enhance the interaction between semantic and visual information. To address the computational burdens caused by jointly training in one-stage methods, iKUN [11] decouples tracker and matcher, developing a modular framework that achieves superior performance compared to end-to-end baselines. However, iKUN’s reliance on CLIP’s [1] dual-tower framework inherently constrains its feature spaces to CLIP-specific visual-textual representations. This design limitation impedes compatibility with emerging visual/text encoders and caps its theoretical potential. Building upon recent advances, TempRMOT [8] constructs the enhanced Refer-KITTI-v2 dataset by leveraging large language models [24], achieving SOTA performance, while its computational overhead still persists and reveals performance bottlenecks in complex scenarios of Refer-KITTI-v2, because it only adopts a simple early-fusion for cross-modal feature integration. Instead, the proposed CPAny leverages a unified

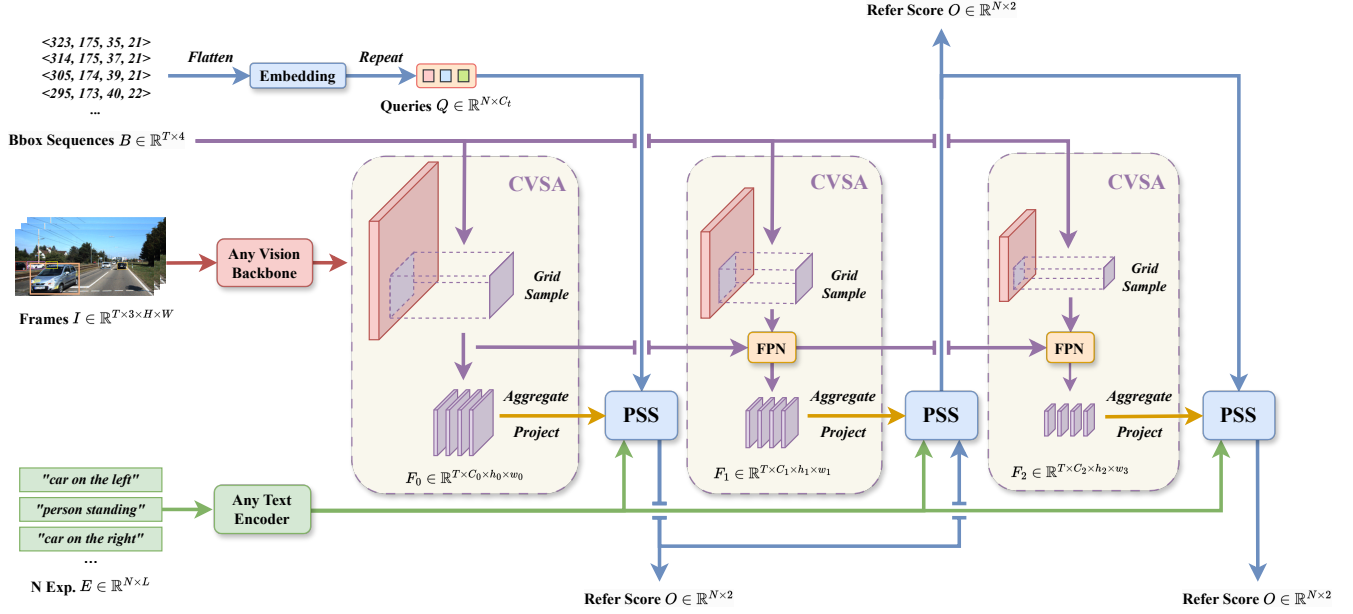


Fig. 3. The overall framework of CPAny. First, the video frames and expressions are processed through the visual backbone and text encoder to form linguistic features and multi-layer visual features. Then, based on the bounding box sequence  $B$ , the proposed CVSA abstracts the targets' features  $F$  from global features and aggregates them to visual semantics. Next, the query vectors  $Q$ , which embed prior knowledge from the bounding box sequence  $B$ , are progressively decoded in the PSS with visual semantic features and linguistic features, ultimately generating the referring scores  $O$ .

semantic space to achieve robust cross-modal information extraction capabilities, and its high flexibility ensures its future-proofing.

### III. METHOD

#### A. Problem Formulation

As a two-stage method, CPAny is typically integrated directly after an off-the-shelf tracker. Each tracked target will be sequentially matched with the given expression by CPAny. For a target in the current frame  $I_t$ , CPAny utilizes its trajectory over the previous  $T - 1$  frames, forming an ordered sequence of  $T$  frames:  $\{I_{t-T+1}, \dots, I_{t-1}, I_t\} \in \mathbb{R}^{T \times 3 \times H \times W}$ . Besides images, CPAny also takes the sequence of bounding box coordinates for the target in each frame as input:  $\{B_{t-T+1}, \dots, B_{t-1}, B_t\} \in \mathbb{R}^{T \times 4}$ , which are directly derived from the tracker. At each step, a set of  $N$  expressions is sampled, and their word-level linguistic features are extracted from the text encoder:  $\{E_1, E_2, \dots, E_N\} \in \mathbb{R}^{N \times L \times C_t}$ , where  $L$  represents the length of the expression. Finally, CPAny outputs a set of logits  $O \in \mathbb{R}^{N \times 2}$ , where each row corresponds to the referring result between one of the  $N$  expressions and the current target.

#### B. The CPAny Framework

As shown in Fig. 3, CPAny consists of four main components: visual backbone, text encoder, Contextual Visual Semantic Abstractor (CVSA), and Parallel Semantic Summarizer (PSS). CPAny first projects the bounding-box sequence using a linear module to generate a set of specialized query vectors  $Q \in \mathbb{R}^{N \times C_t}$ . Subsequently, the query vectors are progressively decoded in the PSS with visual semantic features  $\{J_i \in$

$\mathbb{R}^{C_t \times h_i \times w_i}\}_{i=0}^3$  and linguistic features  $E \in \mathbb{R}^{N \times L}$ , ultimately outputting the referring scores  $\{O_i \in \mathbb{R}^{N \times 2}\}_{i=0}^3$  at each layer  $i$ . The linguistic features are extracted by the text encoder, while the visual semantic features are generated in the CVSA using sampled visual features  $\{F_i \in \mathbb{R}^{T \times C_i \times h_i \times w_i}\}_{i=0}^3$  from outputs of the visual backbones  $\{I_i \in \mathbb{R}^{T \times C_i \times H_i \times W_i}\}_{i=0}^3$ .

#### C. Contextual Visual Semantic Abstractor

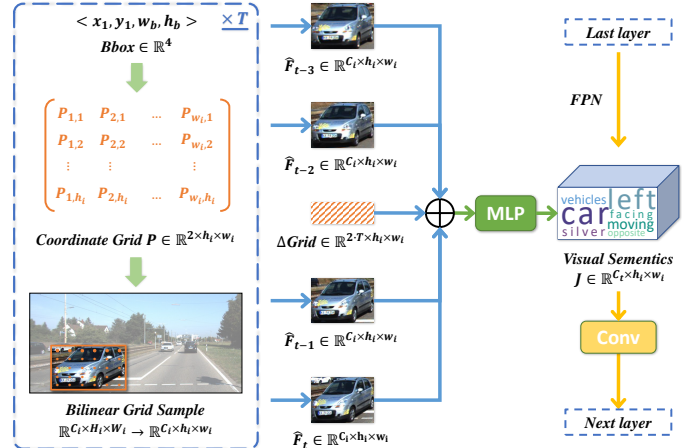


Fig. 4. Illustration of CVSA module. Given a sequence of bounding boxes  $B \in \mathbb{R}^{T \times 4}$ , CVSA first computes coordinate grids  $P \in \mathbb{R}^{2 \times h_i \times w_i}$  and performs bilinear interpolation-based grid sampling on global features, while processing multiple frames simultaneously. For the extracted multi-frame local features  $\{\hat{F}_i \in \mathbb{R}^{C_i \times h_i \times w_i}\}_{i=0}^3$ , CVSA concatenates them along with the channel dimension to form optical flow-like representations, while explicitly incorporating motion cues through inter-frame coordinate grid displacements  $\Delta Grid$ . The composite features are subsequently abstracted into visual semantics via an MLP. Between different layers, CVSA inserts convolutional downsampling to construct a feature pyramid.

In addition to spatially invariant attributes such as color, RMOT involves numerous spatially varying descriptions related to camera perspectives, such as “the car faster than us”. Therefore, neither global visual features nor local cropped features alone are sufficient to accurately characterize a target’s current state. This fundamental limitation requires the model to extract context-aware local visual features, thereby focusing on specific targets while retaining global awareness. To achieve it, existing works usually implement two separate CLIP encoders to process full images and cropped targets respectively, while resulting in computational redundancy. Therefore, by replacing repeated encoding with grid sampling, we design the CVSA shown in Fig. 4 to extract target context features more efficiently and abstract visual semantics used for subsequent summarization of referring scores.

In CVSA, we first convert the input bounding box sequence  $B = \langle x_1, y_1, w_b, h_b \rangle \in \mathbb{R}^4$  into a continuous coordinate grid  $P \in \mathbb{R}^{2 \times h_i \times w_i}$ , where  $(x_1, y_1)$  represents the coordinates of the top-left corner of the target,  $w_b$  and  $h_b$  are the width and height of the bounding box, and  $w_i$  and  $h_i$  represent the width and height of the target features in the  $i$ -th layer. The elements  $P_{i,j}$  in the coordinate grid are calculated as follows:

$$P_{i,j} = P_{1,1} + (i-1) \cdot \Delta x + (j-1) \cdot \Delta y$$

$$\Delta x = \left( \frac{w_b}{w_i}, 0 \right), \Delta y = \left( 0, \frac{h_b}{h_i} \right) \quad (1)$$

where,  $P_{1,1} = (x_1, y_1)$ , and  $\Delta x$  and  $\Delta y$  represent the stride between sampling points. By using the coordinate grid, we extract target features from the global features with bilinear interpolation grid sampling operation in PyTorch [25].

The grid sample operation preserves gradient flow continuity, ensuring that although CVSA only samples features from the target region, gradients can still propagate globally via the backbone network. This makes CVSA naturally capable of contextual understanding and more prominent in the Transformer-based backbone for long-distance modeling.

Coping with the dynamic nature of RMOT that requires simultaneous modeling of static attributes and motion states (e.g., “the car turning left”), CVSA further concatenates multi-frame static features along the channel dimension to form optical flow-like features for extracting motion patterns and obtains the injection of inter-frame motion cues by combining coordinate grid displacements  $\Delta Grid = Cat(\{P_{t-i} - P_{t-i-1}\}_{i=0}^T)$ .  $\Delta Grid$  approximates dense motion fields via coordinate transformations, providing motion priors of the target. The synthesized features and motion cues are then projected into the linguistic embedding space through a multi-layer perceptron (MLP). Moreover, to enhance multi-scale perception, we insert convolutional downsampling layers to construct a feature pyramid network [26] (FPN), enabling adaptive feature resolution matching for diverse tracking targets.

#### D. Parallel Semantic Summarizer

To mitigate the dependency on the modality alignment of encoders and keep future-proofing, we adopt a decoder-based strategy instead of the cosine similarity-based score

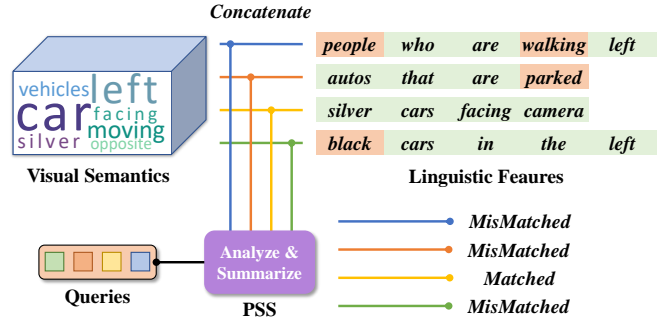


Fig. 5. Illustration of the PSS workflow. Simultaneously referencing visual semantics and linguistic features, PSS performs parallel analysis and summarizes the matching status between the target and multiple expressions.

computation used in the existing methods [11]. As illustrated in Fig. 5, PSS operates on unified semantic representations formed by the concatenation of visual semantics and expression words, working similarly to decoder-based language models [24, 27]. By analyzing and summarizing the visual semantics and linguistic features in parallel, PSS decodes the matching relationship between the target and the expression.

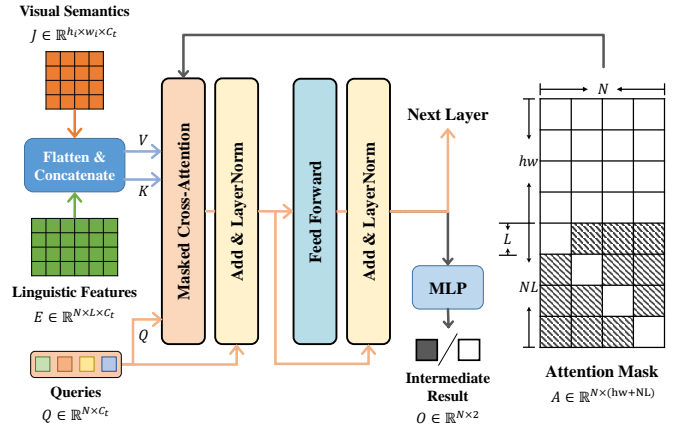


Fig. 6. The structure of PSS. PSS consists of a masked cross-attention, a Feed-Forward Network (FFN), and an MLP with a hidden layer. The attention mask on the right ensures that the query vectors only interact with the corresponding expression, where shaded area and blank area represent the invisible and visible regions respectively.

Specifically, as shown in Fig. 6, after concatenating the visual semantics  $J \in \mathbb{R}^{C_t \times h_i \times w_i}$  and linguistic features  $E \in \mathbb{R}^{N \times L \times C_t}$  in the spatial dimension (the word dimension in  $E$ ), PSS uses them as Key and Value, with the query vectors  $Q \in \mathbb{R}^{N \times C_t}$  as the Query, to perform masked cross-attention. Then, the extracted information is further summarized through a Feed-Forward Network (FFN) followed by an MLP to generate the referring score  $O \in \mathbb{R}^{N \times 2}$ . In the cross-attention mask  $A \in \mathbb{R}^{N \times (h_i \cdot w_i + N \cdot L)}$ , we assign expressions to the query vectors one by one and ensure that the visual semantics are always visible to all query vectors. At each layer, we iteratively decode query vectors from shallow to deep, facilitating the query vectors’ analysis of the target state at different feature granularity.

Unlike existing methods [8, 9, 11], PSS enables dynamic

TABLE I  
COMPARISON WITH STATE-OF-THE-ART METHODS ON REFER-KITTI [7] AND REFER-KITTI-V2 [8]. THE BEST RESULTS ARE IN BOLD.

	Method		HOTA	DetA	AssA	DetRe	DetPr	AssRe	AssPr	LocA	
Refer-KITTI											
One-Stage	EchoTrack [28]		39.47	31.19	51.56	42.65	48.86	56.68	81.21	79.93	
	DeepRMOT [29]		39.55	30.12	53.23	41.91	47.47	58.47	82.16	80.49	
	TransRMOT [7]		46.56	37.97	57.33	49.69	60.10	60.02	89.67	90.33	
	MLS-Track [9]		49.05	40.03	60.25	59.07	54.18	65.12	88.12	-	
	TempRMOT [8]		52.21	40.95	66.75	55.65	59.25	71.82	87.76	90.40	
Two-Stage	FairMOT [30]		22.78	14.43	39.11	16.44	45.48	43.05	71.65	74.77	
	DeepSORT [31]		25.59	19.76	34.31	26.38	36.93	39.55	61.05	71.34	
	ByteTrack [32]		24.95	15.50	43.11	18.25	43.48	48.64	70.72	73.90	
	CStrack [33]		27.91	20.65	39.10	33.76	32.61	43.12	71.82	79.51	
	TransTrack [7]		32.77	23.31	45.71	32.33	42.23	49.99	78.74	79.48	
	TrackFormer [34]		33.26	25.44	45.87	35.21	42.10	50.26	78.92	79.63	
	iKUN [11]		48.84	35.74	66.80	51.97	52.25	72.95	87.09	-	
		CLIP [1]	CLIP-R 50 [1]	52.93	42.36	66.22	60.02	57.64	71.40	88.08	90.82
	CPAny	BERT [13]	ROPE Dei-T-S [35]	48.24	36.72	63.54	56.04	50.31	68.78	87.46	89.51
			Swin-T [12]	51.12	39.85	65.75	59.91	52.94	71.70	86.86	89.58
			Resnet34 [36]	53.15	42.77	66.23	59.00	<b>59.12</b>	72.00	87.16	89.72
ROPE Swin-T [35]			53.30	42.44	67.13	<b>63.29</b>	54.74	74.04	86.20	89.46	
RoBERTa [37]	ROPE Dei-T-S [35]	49.08	36.63	65.85	59.55	47.79	71.41	87.75	90.57		
	Swin-T [12]	51.03	39.50	65.99	56.33	55.72	70.49	<b>88.94</b>	<b>90.98</b>		
	Resnet34 [36]	53.28	41.89	<b>67.87</b>	63.18	54.20	<b>74.08</b>	87.35	90.75		
	ROPE Swin-T [35]	<b>53.83</b>	<b>43.40</b>	66.86	60.98	58.69	72.26	88.07	90.85		
Refer-KITTI-V2											
One-Stage	TransRMOT [7]		31.00	19.40	49.68	36.41	28.97	54.59	82.29	89.82	
	TempRMOT [8]		35.04	22.97	53.58	34.23	40.41	59.50	81.29	<b>90.07</b>	
Two-Stage	FairMOT [30]		22.53	15.80	32.82	20.60	37.03	36.21	71.94	78.28	
	ByteTrack [32]		24.59	16.78	36.63	22.60	36.18	41.00	69.63	78.00	
	iKUN [11]		10.32	2.17	49.77	2.36	19.75	58.48	68.64	74.56	
		CLIP [1]	CLIP-R 50 [1]	41.44	28.71	<b>59.95</b>	<b>61.68</b>	34.32	<b>66.31</b>	84.45	89.12
	CPAny	BERT [13]	ROPE Dei-T-S [35]	39.63	27.20	57.86	58.30	33.17	63.13	85.15	89.03
			Swin-T [12]	41.14	28.78	58.94	59.63	35.06	64.91	84.51	88.97
			Resnet34 [36]	41.04	29.24	57.76	56.19	37.14	62.97	85.35	89.19
			ROPE Swin-T [35]	41.16	29.41	57.76	51.77	39.72	63.32	85.52	89.52
	RoBERTa [37]	ROPE Dei-T-S [35]	39.14	26.61	57.68	59.23	32.02	63.44	84.45	88.97	
		Swin-T [12]	40.32	27.47	59.29	60.09	33.00	65.19	84.72	88.96	
		Resnet34 [36]	41.71	30.07	57.99	54.56	39.30	62.80	<b>85.91</b>	89.25	
ROPE Swin-T [35]		<b>42.81</b>	<b>31.35</b>	58.61	55.89	<b>40.77</b>	63.78	85.71	89.22		

assessment of semantic alignment between input pairs and shifts from static similarity measurement to an active reasoning process. On the one hand, compared with serial processing in current methods, PSS enables explicit contrastive learning between matched and mismatched sample pairs and improves inference efficiency. On the other hand, by avoiding the inevitable information loss in early-fusion of one-stage methods [7], PSS directly decodes raw linguistic features and visual semantics, effectively discriminating the subtle differences in the dense semantic space.

### E. Loss Computation

To enhance the stability of the output and align with the pre-trained model, we employ the multi-class cross-entropy

loss, as shown in Equation 2 for supervision.

$$l_{ce} = \log \frac{\exp(O_{n,y_n})}{\sum_{c=1}^C \exp(O_{n,c})} \quad (2)$$

where,  $C$  is the number of classes, which is 2 in CPAny.  $y_n$  represents the true label of the current sample pair.  $O_{n,c}$  refers to the  $c$ -th channel of the current result  $O_n$ .

However, the naive cross-entropy loss is not sufficient to address the fundamental challenges arising from data distribution in two-stage RMOT. These challenges manifest through 3 primary issues: 1) Semantic complexity disparity between simple expressions (e.g., “left car”) and complex expressions (e.g., “woman with a backpack”) creates unequal feature representation difficulty. 2) Complex expressions, being inherently more specific, lead to sparser matching targets and aggravate the long-tail distribution problem. 3) Lost targets arising from

detector inaccuracies are naturally viewed as false negatives throughout the inference, introducing systemic errors.

Therefore, inspired by Focal Loss [26], we enhance the multi-class cross-entropy loss by incorporating hard sample mining (for issue 1) and balancing between positive and negative examples (for issues 2-3) as follows:

$$L = - \sum_N [\alpha \cdot y_n + (1 - \alpha)(1 - y_n)] \cdot l_h \quad (3)$$

where,  $\alpha$  is used to balance recall and precision, while  $l_h$  is used for hard sample mining, and its calculation is as follows:

$$l_h = l_{ce} \cdot \text{detach}(h_n^\beta) \quad (4)$$

$$h_n = - \sum_{c=1}^C p(O_{n,c}) \log p(O_{n,c})$$

where,  $h_n$  is the information entropy of prediction and  $\beta$  is used to control its strength. `detach` refers to the ‘‘detach’’ operation in PyTorch, which removes  $h_n$  from the computation graph to prevent it from affecting the back-propagation.

## IV. EXPERIMENT

### A. Experiment Setup

**Dataset and Metrics.** We evaluate the proposed framework on the only two widely used RMOT datasets currently available: Refer-KITTI [7] and Refer-KITTI-V2 [8]. For the Refer-KITTI training set, we employ a small subset of labels from Refer-KITTI-V2 to correct the original annotations, without data leakage, new words, or additional objects. For a fair comparison, we use Higher Order Tracking Accuracy [38] (HOTA) as the main evaluation metric, following TransRMOT [7]. HOTA comprehensively considers the detection and association capabilities of the tracking model. We also report the localization accuracy (LocA), the detection accuracy (DetA) and the association accuracy (AssA) with their corresponding recall and precision. Further details can be found in the Supplemental Material.

**Implement Details.** We use multiple visual backbones and text encoders to verify the strong adaptability of our model to any encoder. The visual backbones used include ResNet [36], DeiT [39, 40], Swin [12, 41], and RoPE Swin [35], all of which use the pre-trained parameters on ImageNet [42], with an input size of  $224 \times 672$  to align as closely as possible with the aspect ratio of KITTI [43]. For text encoders, we test both RoBERTa [37] and BERT [13].

In each epoch, we iterate over all frames of all targets, with sample stride 2, and each sample consists of 4 frames. During inference, the sample stride is set to 1. In each training iteration, each target is coupled with 8 randomly sampled expressions, among which 4 ones are positive and 4 ones are negative. We use AdamW [44] as the optimizer, with a learning rate of  $3e-5$ , and train for 20 epochs. But in many cases, CPAny only requires 10 epochs to achieve good performance. All experiments are performed on two NVIDIA 4090 GPUs.

### B. Benchmark Experiments

We compare our method with SOTA approaches on Refer-KITTI and Refer-KITTI-V2 in Table I. Since switching trackers does not require retraining, we report only the results for the best detector & tracker: TempRMOT [8] & NeuralSORT [11]. As a detector, TempRMOT is trained using detection labels, in which we treat each target in each frame as a new target. Structurally, TempRMOT as a detector can be seen as a DeformableDETR [45] with added inter-frame interactions. More results of other trackers [11, 45–47] can be found in the Supplemental Material.

Compared to the current SOTA method TempRMOT, our best model, CPAny+RoBERTa [37]+ROPE Swin-T [35], achieves superior performance on both Refer-KITTI and Refer-KITTI-V2, surpassing TempRMOT by 7.77%, 8.38%, and 5.03% on HOTA, DetA, and AssA, respectively. CPAny particularly exhibits significant advantages in HOTA and DetA, demonstrating its powerful matching capability, especially on the complex Refer-KITTI-V2 dataset.

Among the different combinations, the best text encoder is RoBERTa [37], followed by CLIP [1], while the best visual backbone is ROPE Swin-T [35], followed by Resnet34 [36]. The performance of CPAny with the naive Swin-T model is not as good, suggesting that rotational position encoding plays a significant role in extracting target attributes. DeiT [39] generally performs poorly, mainly due to the coarser granularity of its features. We also evaluate the coupling effectiveness of CPAny with CLIP [1] encoder pairs following iKUN [11]. The results demonstrate that even beyond CLIP, numerous visual/text encoders can achieve superior performance. This highlights the critical importance of CPAny’s future-proofing capability in adapting to evolving encoders.

### C. Ablation Study

**Contextual Visual Semantic Abstractor.** In addition to the MLP, we design two other feature aggregation strategies for CVSA for comparison. (a) Conv strategy: Similar to MLP, but uses 2D convolution to aggregate the features instead; (b) Attention strategy: Concatenate the features along the spatial dimension followed by a self-attention module, after which they are concatenated along the channel dimension and aggregated using a linear layer.

TABLE II  
PERFORMANCE COMPARISON OF DIFFERENT AGGREGATES STRATEGIES IN CVSA.

Strategy	HOTA	DetA	AssA
Attention	41.38	29.76	57.69
Conv	41.90	29.79	<b>59.06</b>
MLP	<b>42.82</b>	<b>31.35</b>	58.61

As shown in Table II, it seems that more complex aggregation methods perform even worse than the simple MLP-based approach. This can be attributed to the fact that pre-trained visual backbones already encode rich static information within each sampled frame. Complex aggregation strategies may

distort feature representations, making subsequent learning more difficult.

TABLE III  
COMPARISON OF THE PERFORMANCE BETWEEN VARIOUS SEQUENTIAL DECODING AND PSS.

	$Q_1$	$KV_1$	$Q_2$	$KV_2$	HOTA	DetA	AssA
#1	Q	L	Q	V	40.55	27.81	59.25
#2	Q	V	Q	L	40.94	28.31	59.35
#3	V	L	Q	V	40.85	29.56	56.59
#4	L	V	Q	L	41.40	29.39	58.46
	PSS				<b>42.82</b>	<b>31.35</b>	<b>58.61</b>

**Parallel Semantic Summarizer.** In Table III, we investigate the performance of the PSS. For comparison, we design four Transformer-based decoding structures, all of which adopt a sequential decoding strategy similar to existing one-stage methods, consisting of two sets of cross-attention layers. They interact between visual features, textual features, and query vectors in different sequences and combinations.

Here, Q, L and V represent the query vectors, linguistic features and visual semantics respectively. Before calculating referring scores using the query vectors, interacting with linguistic features yields better results than interacting with visual features, as evidenced by the comparisons between #1 & #3 and #2 & #4. Furthermore, when comparing #3 and #4, it can be seen that integrating sparse visual semantics into the dense textual space achieves superior performance compared to using the visual space as the base space. However, regardless of how the order of cross-attention interactions is arranged, sequential decoding consistently performs worse than parallel decoding in PSS.

TABLE IV  
IMPACT OF PARAMETER IN THE LOSS FUNCTION.

$\alpha$	$\beta$	HOTA	DetA	AssA	DetRe	DetPr
0.3	1	40.11	29.50	54.72	46.15	<b>44.03</b>
0.5	1	41.03	29.68	56.86	46.64	44.01
<b>0.7</b>	<b>1</b>	<b>42.81</b>	<b>31.35</b>	58.61	55.89	40.77
0.9	1	41.27	28.58	<b>59.72</b>	<b>61.75</b>	34.10
0.7	0	41.25	29.08	58.64	57.24	36.45
0.7	2	41.96	30.61	57.67	55.46	39.72

**Loss Parameter.** In Table IV, we evaluate the effects of different values of  $\alpha$  and  $\beta$ , which are used to balance recall and precision and control the weighting strength of hard samples, respectively.  $\alpha$  performs better when it is greater than 0.5, but when the recall is too high, the performance starts to degrade. Therefore, we select 0.7 as the optimal value for  $\alpha$ . Additionally, when  $\alpha$  is fixed at 0.7, we vary the value of  $\beta$ . It can be observed that the weight for hard samples should neither be absent ( $\beta = 0$ ) nor excessive. The highest HOTA is achieved when  $\beta$  is set to 1.

**Training and inference time.** Table V shows a comparison of training and inference time, where the combination of CPAny is RoBERTa [37] + ROPE Swin-T [35]. iKUN [11] follows the official configuration, sampling only 4 frames per trajectory

TABLE V  
COMPARISON OF TRAINING AND INFERENCE TIME. ALL EXPERIMENTS ARE CONDUCTED ON 2 NVIDIA 4090 GPUS ON REFER-KITTI-V2 [8].  
“†” : iKUN [11] TRAINS AT THE TRAJECTORY LEVEL.

Method	Epoch	Train	Inference	HOTA
TempRMOT [8]	50	62 h	299 min	35.04
iKUN† [11]	100	2.51 h	115 min	10.32
CPAny	20	2.17 h	27 min	42.82

in each training epoch and employing a frame sampling stride of 4 during inference, which leads to a notable variance in total epochs. However, benefiting from redundancy reduction and parallel inference, CPAny still demonstrates a significant efficiency advantage, even with frame-by-frame processing.

#### D. Qualitative Results

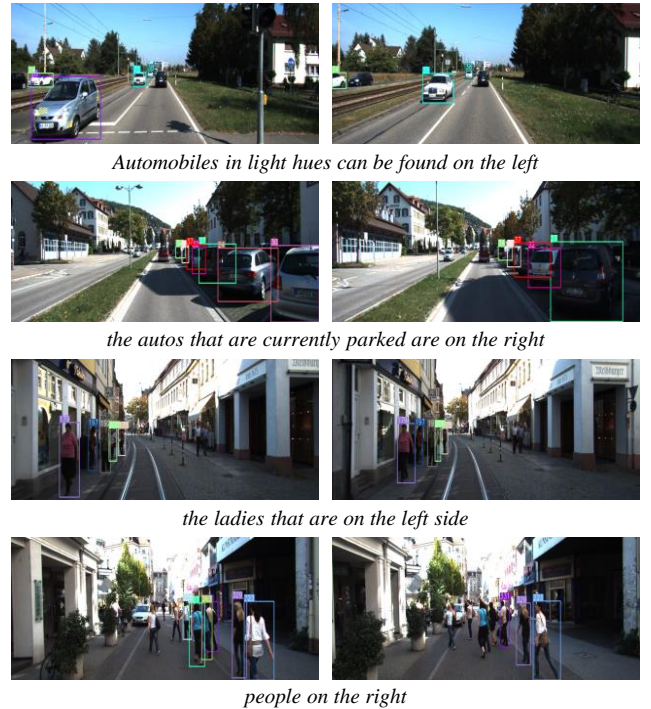


Fig. 7. Visualization of some qualitative results.

We visualize several typical referring results in Fig. 7 and the Supplementary Material. In the first expression, CPAny effectively distinguishes between light-colored and dark-colored vehicles and accurately understands the target’s location. In the second expression, despite the continuous movement of the visual capture, CPAny still accurately identifies that the vehicles on the right are stationary. The third expression is more complex, involving both the target’s location and gender. The final expression highlights CPAny’s adjustment in matching the target during movement. In the video, a group of pedestrians crosses the road, but the expression only describes pedestrians on the right side. As soon as the target reaches the center or shifts slightly to the left, CPAny cancels the match.

## V. CONCLUSION

In this work, we address the limitations of existing two-stage RMOT methods [11] by proposing CPAny, a flexible and efficient encoder-decoder framework. CPAny introduces two novel components, CVSA and PSS, which enable context-aware feature aggregation and parallel semantic decoding, achieving significant gains in accuracy and computational efficiency. By projecting visual features into a unified semantic space, CPAny circumvents the dependency on intrinsic encoder modal alignment while demonstrating exceptional adaptability to various emerging visual/text encoders and ensuring future-proofing.

# Supplementary Material

## I. DATASET DETAILS

**Refer-KITTI.** Refer-KITTI [15] uses 18 low-complexity videos and tracking annotations from the KITTI [43] training set, encompassing a total of 895 expressions [8]. During the annotation process, manual bidirectional verification is performed on the matching between expressions and targets to ensure annotation accuracy. Although Refer-KITTI lays the foundation for RMOT, its test set is relatively small and exhibits a significant distribution gap from the training set, resulting in a failure to accurately reflect real-world scenarios [8].

**Refer-KITTI-V2.** Recognizing the issues in Refer-KITTI, Refer-KITTI-V2 [8] leverages large language models to further enrich the diversity of expressions in Refer-KITTI. Building on the 18 videos from Refer-KITTI, Refer-KITTI-V2 includes 9758 expressions and an additional 3 videos from the KITTI [43] training set, with 2 used for training and 1 for testing. The diversified expressions and more complex scenarios make Refer-KITTI-V2 more reflective of real-world conditions compared to Refer-KITTI, presenting new challenges for RMOT.

**Correction strategy of Refer-KITTI.** Refer-KITTI has suffered from multiple annotation errors for a long time. Many critical issues like frame misalignment have been addressed in iKUN [11] and Refer-KITTI-V2 [8]. However, the problem of incomplete reference persists in the current version. For instance, in frames 231-232 of video “0002”, two silver vehicles are referenced under the label “left cars in light color” but are missing in the “left-cars-in-silver”. Furthermore, numerous objects originally annotated in the KITTI [43] tracking dataset, such as all pedestrians in video “0001”, are entirely omitted in Refer-KITTI.

Compared to one-stage methods that use all tracking annotations for training, the two-stage methods based on pairwise sample training have only negative examples without any positive ones in many targets due to the above issues, which leads to particularly significant adverse effects. For a fair comparison, we select expressions from Refer-KITTI-V2 that consist solely of words previously used in Refer-KITTI and replace the original annotations with them, thereby resolving the existing issues in Refer-KITTI without introducing new words or causing data leakage. To verify the rationality of our correction strategy, we retrain TempRMOT [8] using the corrected Refer-KITTI dataset. As shown in Table VI, our correction strategy does not benefit the one-stage methods, since TempRMOT itself already utilizes all the tracking annotations.

TABLE VI  
PERFORMANCE COMPARISON OF TEMP<sub>RMOT</sub> [8] BEFORE AND AFTER THE CORRECTION OF REFER-KITTI [7].

Correction	HOTA	DetA	AssA
Before	52.21	40.95	66.75
After	51.79	40.28	66.68

TABLE VII  
COMPARISON OF IKUN’S [11] PERFORMANCE WHEN COUPLED WITH DIFFERENT ENCODERS ON REFER-KITTI [7].

Visual Backbone	Text Encoder	HOTA	DetA	AssA
ROPE Swin [35]	RoBERTa [37]	29.79	14.73	60.38
ROPE Swin [35]	RoBERTa <sup>†</sup> [37]	46.23	32.20	66.47
CLIP [1]	CLIP [1]	48.84	35.74	66.80

## II. THE ADAPTABILITY OF IKUN

Following the official configuration of iKUN [11], we evaluate its performance when coupled with other encoders in Table VII to explore the adaptability of the current two-stage methods. Here, ROPE Swin [35] uses the tiny version, CLIP [1] adopts the ResNet50 version following iKUN [11], and <sup>†</sup> indicates that the text encoder is trainable in this experiment (iKUN’s official configuration requires freezing the text encoder). It is evident that when using the best encoder combination in CPAny (i.e., ROPE Swin-T [35] & RoBERTa [37]), iKUN [11] fails to fully leverage the capabilities of advanced encoders, as CPAny does. Particularly when freezing and controlling the feature space to the linguistic feature space, iKUN’s performance significantly declines, and even after unfreezing the text encoder, no performance improvement is observed. This indicates that iKUN heavily depends on encoder pairs with inherent feature alignment capabilities, such as CLIP [1], and struggles to integrate with emerging encoders, making it not capable of future proofing.

## III. THE SCALABILITY OF CPANY

In Table IX, we evaluate the performance of CPAny with different sizes of ResNet [36] and RoPE Swin Transformer [35] as visual backbones. The text encoder maintains RoBERTa [37]. It can be observed that as the size of the Swin Transformer increases, the performance of CPAny does not improve significantly and even decreases. However, for convolutional networks, as the size of ResNet increases, the performance of CPAny continues to improve, but this improvement stops at ResNet34. This indicates that the scalability of visual backbones of different sizes for CPAny is not significant, but CNN-based backbones slightly outperform Transformer-based ones. This can be attributed to the limited visual information of most targets in the current Refer-KITTI-V2 dataset, which does not require a very powerful visual backbone to characterize the target’s state. When the visual backbone is too powerful, the model is more prone to overfitting. Therefore, we ultimately selected ResNet34 and ROPE Swin-T for reporting.

## IV. IMPACT OF FREEZING

In Table X, we evaluate the impact of freezing different components in CPAny, where CPAny+CLIP represents the CLIP-R 50 [1] encoder pair, and CPAny+Best refers to the ROPE Swin-T [35] + RoBERTa [37] encoder pair. It is observed that freezing the text encoder has a more significant negative effect compared to freezing the visual backbone. This is primarily due to the fact that the proposed CVSA has the

TABLE VIII  
PERFORMANCE COMPARISON OF MULTI-OBJECT TRACKING ON KITTI [43] (USING THE SAME SPLIT AS TEMPRMOT [8]).

	Detector	Tracker	HOTA	DetA	AssA	DetRe	DetPr	AssRe	AssPr	LocA
One-stage	TempRMOT [8]		<b>63.47</b>	56.09	<b>72.04</b>	61.56	83.68	<b>76.07</b>	89.67	<b>91.19</b>
Two-stage	D-DETR [45]	OC-SORT [46]	54.13	50.31	58.46	53.39	<b>86.42</b>	61.39	88.19	90.73
		StrongSORT [47]	56.98	54.13	60.20	58.54	84.29	62.72	<b>90.70</b>	90.24
		NeuralSORT [11]	56.84	54.37	59.67	59.62	82.57	63.31	88.41	89.89
	TempRMOT [8]	OC-SORT [46]	58.26	55.35	61.57	61.51	81.48	65.30	86.09	90.44
		StrongSORT [47]	59.42	57.25	61.92	65.69	78.42	66.68	86.50	89.91
		NeuralSORT [11]	61.10	<b>57.56</b>	65.08	<b>66.36</b>	78.04	69.26	88.27	89.84

TABLE IX  
COMPARISON OF CPANY PERFORMANCE WITH DIFFERENT-SIZED VISUAL ENCODERS ON REFER-KITTI-V2 [8].

Backbone	Size	HOTA	DetA	AssA
ROPE Swin [35]	Tiny	<b>42.81</b>	<b>31.35</b>	<b>58.61</b>
	Small	41.50	28.76	60.05
	Base	41.16	29.43	57.70
ResNet [36]	18	40.99	28.89	58.31
	34	<b>41.71</b>	<b>30.07</b>	<b>57.99</b>
	50	40.61	27.85	59.36

TABLE X  
PERFORMANCE OF CPANY AFTER FREEZING DIFFERENT MODULES ON REFER-KITTI-V2 [8].

Method	Visual Backbone	Text Encoder	HOTA	DetA	AssA
CPAny +CLIP	Trainable	Frozen	40.76	28.93	57.57
	Frozen	Trainable	41.17	<b>29.48</b>	57.65
	Frozen	Frozen	40.92	29.07	57.75
	Trainable	Trainable	<b>41.44</b>	28.71	<b>59.95</b>
CPAny +Best	Trainable	Frozen	40.44	28.09	58.38
	Frozen	Trainable	41.05	29.73	56.81
	Frozen	Frozen	40.55	28.60	57.62
	Trainable	Trainable	<b>42.81</b>	<b>31.35</b>	<b>58.61</b>

ability to abstract visual features into semantic representations. As a result, freezing the visual backbone does not significantly impede the construction of the unified semantic space. In contrast, freezing the text encoder forces the unified semantic space to align solely with the text encoder’s feature space. The limited training samples are insufficient for the CVSA to fully project visual features into linguistic feature space, resulting in performance degradation.

Additionally, freezing other encoders has a more pronounced negative impact compared to the CLIP encoders, indicating that CLIP’s inherent modality alignment effectively reduces the difficulty of constructing a unified semantic space. However, training both encoders simultaneously to align bidirectionally the feature spaces of the two modalities consistently proves to be more beneficial.

## V. PERFORMANCE OF OTHER TRACKER

As a two-stage RMOT method, the proposed CPAny can also couple with arbitrary trackers, achieving seamless inte-

gration with any tracker, any visual backbone, and any text encoder. In Table VIII, we compare the multi-object tracking performance of various detector / tracker combinations used in our approach with the one-stage method TempRMOT [8]. Here, "D-DETR" refers to DeformableDETR [45]. In the two-stage method, TempRMOT [8] serves solely as a detector and adheres to the detection paradigm, where we treat each target in each frame as a new addition. Overall, even when employing tracking models weaker than those in the one-stage method, CPAny still outperforms the current SOTA method TempRMOT [8] in RMOT tasks, as shown in Table XI. This demonstrates that CPAny significantly surpasses TempRMOT in matching capability, providing excellent results even when coupled with inferior trackers. Additionally, in Table VIII and Table XI, CPAny achieves consistent performance improvements across various encoder combinations as the capability of the detectors / trackers increases, highlighting its flexibility and robustness.

## VI. MORE QUALITATIVE RESULTS

We visualize additional qualitative results in Fig. 8 and Fig. 9 to provide an intuitive comparison between CPAny and TempRMOT [8], where CPAny employs the encoder combination of ROPE Swin-T [35] + RoBERTa [37]. Here, (a) represents the results of TempRMOT [8], (b) represents the results of CPAny, GT denotes the ground truth, and  $T_1$ ,  $T_2$ , and  $T_3$  correspond to 3 sequentially sampled frames (which are not consecutive). In various scenarios, CPAny has demonstrated robust advantages, showing fewer error cases and lost cases compared to TempRMOT [8].

TABLE XI

PERFORMANCE COMPARISON OF CPANY COUPLED WITH DIFFERENT TRACKERS, VISUAL BACKBONES, AND TEXT ENCODERS ON REFER-KITTI-V2 [8].

Detector & Tracker	Text Encoder	Visual Backbone	HOTA	DetA	AssA	DetRe	DetPr	AssRe	AssPr	LocA
TempRMOT [8]			35.04	22.97	53.58	34.23	40.41	59.50	81.29	90.07
D-DETR [45] & OC-SORT [46]	BERT [13]	ROPE DeiT-S [35]	36.07	25.83	50.51	46.06	36.42	55.29	82.85	89.66
		Swin-T [12]	37.56	27.43	51.58	46.69	39.21	56.87	82.81	89.70
		Resnet34 [36]	37.83	27.95	51.36	45.11	41.58	55.88	83.88	89.92
		ROPE Swin-T [35]	37.91	27.57	52.28	41.54	44.22	56.69	85.23	<b>90.28</b>
	RoBERTa [37]	ROPE DeiT-S [35]	35.91	25.71	50.29	46.54	35.88	55.33	82.92	89.67
		Swin-T [12]	37.38	26.84	52.20	47.32	37.60	57.30	83.33	89.73
		Resnet34 [36]	38.05	28.22	51.45	43.30	43.88	55.32	85.01	89.96
		ROPE Swin-T [35]	38.74	29.08	51.77	44.12	<b>45.10</b>	56.20	84.49	89.97
D-DETR [45] & StrongSORT [47]	BERT [13]	ROPE DeiT-S [35]	37.72	26.88	53.06	50.84	35.68	57.15	86.57	89.30
		Swin-T [12]	39.28	28.50	54.27	51.56	38.18	58.94	86.31	89.31
		Resnet34 [36]	38.44	28.43	52.12	46.71	41.28	55.85	87.22	89.89
		ROPE Swin-T [35]	38.13	28.01	52.03	42.95	43.80	56.03	87.42	90.23
	RoBERTa [37]	ROPE DeiT-S [35]	37.43	26.61	52.80	51.41	34.93	57.16	86.38	89.31
		Swin-T [12]	38.95	27.73	54.83	52.22	36.48	59.36	86.65	89.32
		Resnet34 [36]	38.60	28.72	52.03	44.84	43.53	55.31	<b>87.82</b>	89.92
		ROPE Swin-T [35]	39.26	29.63	52.16	45.73	44.77	55.84	87.62	89.93
D-DETR [45] & NeuralSORT [11]	BERT [13]	ROPE DeiT-S [35]	37.58	26.68	53.08	51.82	34.84	58.17	84.64	88.94
		Swin-T [12]	38.88	28.31	53.58	52.54	37.30	59.35	84.18	88.94
		Resnet34 [36]	39.27	28.83	53.65	50.25	39.55	58.48	85.52	89.26
		ROPE Swin-T [35]	39.27	28.61	54.07	46.09	42.16	58.71	86.31	89.58
	RoBERTa [37]	ROPE DeiT-S [35]	37.38	26.43	53.01	52.42	34.15	58.23	84.55	88.93
		Swin-T [12]	38.58	27.51	54.27	53.17	35.62	59.93	84.46	88.95
		Resnet34 [36]	39.63	29.38	53.61	48.45	41.85	57.94	86.15	89.24
		ROPE Swin-T [35]	40.10	30.30	53.25	49.57	42.85	58.15	85.49	89.17
TempRMOT [8] & OC-SORT [46]	BERT [13]	ROPE DeiT-S [35]	37.54	27.03	52.29	53.83	34.59	58.01	80.65	89.47
		Swin-T [12]	39.01	28.62	53.36	54.87	36.73	59.66	80.42	89.44
		Resnet34 [36]	39.15	28.97	53.10	51.96	38.83	58.51	81.63	89.66
		ROPE Swin-T [35]	39.45	29.04	53.75	47.90	41.66	58.95	82.90	90.01
	RoBERTa [37]	ROPE DeiT-S [35]	37.12	26.52	52.10	54.55	33.47	58.22	80.30	89.43
		Swin-T [12]	38.32	27.49	53.58	55.33	34.72	59.58	80.89	89.45
		Resnet34 [36]	39.81	29.67	53.58	50.38	41.08	58.30	82.84	89.69
		ROPE Swin-T [35]	40.56	30.80	53.59	51.54	42.45	58.87	82.20	89.69
TempRMOT [8] & StrongSORT [47]	BERT [13]	ROPE DeiT-S [35]	39.07	27.28	56.08	57.90	33.43	61.80	84.69	89.13
		Swin-T [12]	40.54	28.83	57.18	59.21	35.30	63.58	84.12	89.07
		Resnet34 [36]	40.02	29.16	55.09	53.05	38.57	59.37	86.72	89.64
		ROPE Swin-T [35]	39.98	29.16	54.98	48.77	41.26	59.46	87.12	90.01
	RoBERTa [37]	ROPE DeiT-S [35]	38.61	26.66	56.05	58.79	32.24	62.10	84.13	89.08
		Swin-T [12]	39.77	27.53	57.58	59.64	33.24	63.83	84.42	89.08
		Resnet34 [36]	40.58	29.83	55.34	51.40	40.73	59.16	87.33	89.69
		ROPE Swin-T [35]	41.51	31.02	55.70	52.64	42.15	59.83	87.28	89.68
TempRMOT [8] & NeuralSORT [11]	BERT [13]	ROPE DeiT-S [35]	39.63	27.20	57.86	58.30	33.17	63.13	85.15	89.03
		Swin-T [12]	41.14	28.78	58.94	59.63	35.06	64.91	84.51	88.97
		Resnet34 [36]	41.04	29.24	57.76	56.19	37.14	62.97	85.35	89.19
		ROPE Swin-T [35]	41.16	29.41	57.76	51.77	39.72	63.32	85.52	89.52
	RoBERTa [37]	ROPE DeiT-S [35]	39.14	26.61	57.68	59.23	32.02	63.44	84.45	88.97
		Swin-T [12]	40.32	27.47	<b>59.29</b>	<b>60.09</b>	33.00	<b>65.19</b>	84.72	88.96
		Resnet34 [36]	41.71	30.07	57.99	54.56	39.30	62.80	85.91	89.25
		ROPE Swin-T [35]	<b>42.81</b>	<b>31.35</b>	58.61	55.89	40.77	63.78	85.71	89.22

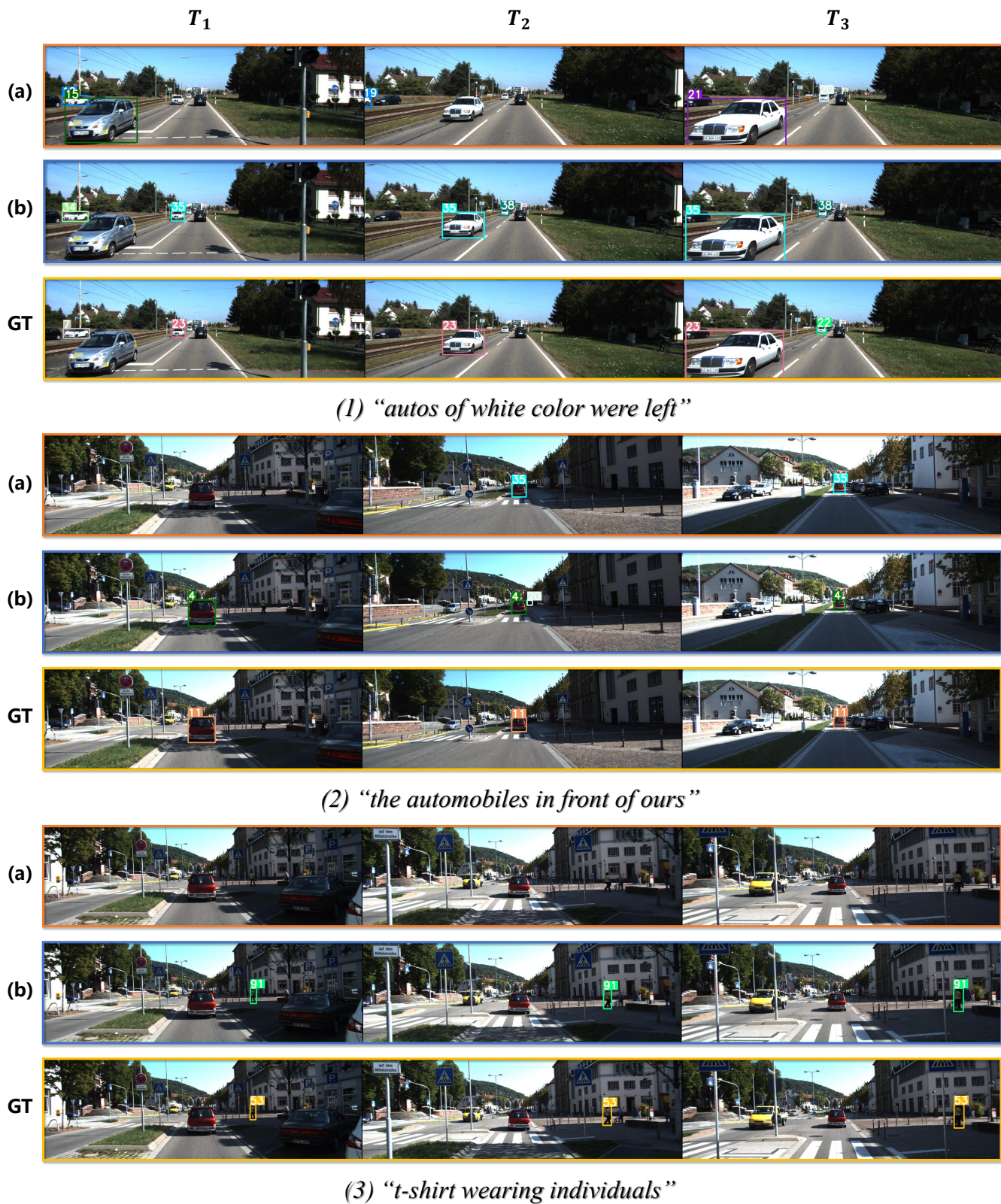


Fig. 8. Visualization of some qualitative results (Part 1).



(4) "those located on the right"



(5) "people on the left"



(6) "the ladies that are on the left side"

Fig. 9. Visualization of some qualitative results (Part 2).

## REFERENCES

- [1] A. Radford, J. W. Kim, C. Hallacy, A. Ramesh, G. Goh, S. Agarwal, G. Sastry, A. Askell, P. Mishkin, J. Clark, G. Krueger, and I. Sutskever, “Learning transferable visual models from natural language supervision,” in *Proceedings of the 38th International Conference on Machine Learning*, ser. Proceedings of Machine Learning Research, M. Meila and T. Zhang, Eds., vol. 139. PMLR, 18–24 Jul 2021, pp. 8748–8763. [Online]. Available: <https://proceedings.mlr.press/v139/radford21a.html>
- [2] J. Li, R. Selvaraju, A. Gotmare, S. Joty, C. Xiong, and S. C. H. Hoi, “Align before fuse: Vision and language representation learning with momentum distillation,” in *Advances in Neural Information Processing Systems*, M. Ranzato, A. Beygelzimer, Y. Dauphin, P. Liang, and J. W. Vaughan, Eds., vol. 34. Curran Associates, Inc., 2021, pp. 9694–9705. [Online]. Available: [https://proceedings.neurips.cc/paper\\_files/paper/2021/file/505259756244493872b7709a8a01b536-Paper.pdf](https://proceedings.neurips.cc/paper_files/paper/2021/file/505259756244493872b7709a8a01b536-Paper.pdf)
- [3] C. Schuhmann, R. Vencu, R. Beaumont, R. Kaczmarczyk, C. Mullis, A. Katta, T. Coombes, J. Jitsev, and A. Komatsuzaki, “Laion-400m: Open dataset of clip-filtered 400 million image-text pairs,” 2021. [Online]. Available: <https://arxiv.org/abs/2111.02114>
- [4] H. Fan, L. Lin, F. Yang, P. Chu, G. Deng, S. Yu, H. Bai, Y. Xu, C. Liao, and H. Ling, “Lasot: A high-quality benchmark for large-scale single object tracking,” in *Proceedings of the IEEE/CVF Conference on Computer Vision and Pattern Recognition (CVPR)*, June 2019.
- [5] L. Huang, X. Zhao, and K. Huang, “Got-10k: A large high-diversity benchmark for generic object tracking in the wild,” *IEEE Transactions on Pattern Analysis and Machine Intelligence*, vol. 43, no. 5, pp. 1562–1577, 2021.
- [6] Y. Wu, J. Lim, and M.-H. Yang, “Online object tracking: A benchmark,” in *Proceedings of the IEEE Conference on Computer Vision and Pattern Recognition (CVPR)*, June 2013.
- [7] D. Wu, W. Han, T. Wang, X. Dong, X. Zhang, and J. Shen, “Referring multi-object tracking,” in *Proceedings of the IEEE/CVF Conference on Computer Vision and Pattern Recognition (CVPR)*, June 2023, pp. 14 633–14 642.
- [8] Y. Zhang, D. Wu, W. Han, and X. Dong, “Bootstrapping referring multi-object tracking,” 2024. [Online]. Available: <https://arxiv.org/abs/2406.05039>
- [9] Z. Ma, S. Yang, Z. Cui, Z. Zhao, F. Su, D. Liu, and J. Wang, “Mls-track: Multilevel semantic interaction in rmot,” 2024. [Online]. Available: <https://arxiv.org/abs/2404.12031>
- [10] F. Zeng, B. Dong, Y. Zhang, T. Wang, X. Zhang, and Y. Wei, “Motr: End-to-end multiple-object tracking with transformer,” in *Computer Vision – ECCV 2022*, S. Avidan, G. Brostow, M. Cissé, G. M. Farinella, and T. Hassner, Eds. Cham: Springer Nature Switzerland, 2022, pp. 659–675.
- [11] Y. Du, C. Lei, Z. Zhao, and F. Su, “ikun: Speak to trackers without retraining,” in *Proceedings of the IEEE/CVF Conference on Computer Vision and Pattern Recognition (CVPR)*, June 2024, pp. 19 135–19 144.
- [12] Z. Liu, Y. Lin, Y. Cao, H. Hu, Y. Wei, Z. Zhang, S. Lin, and B. Guo, “Swin transformer: Hierarchical vision transformer using shifted windows,” in *Proceedings of the IEEE/CVF International Conference on Computer Vision (ICCV)*, October 2021, pp. 10 012–10 022.
- [13] J. Devlin, M.-W. Chang, K. Lee, and K. Toutanova, “BERT: Pre-training of deep bidirectional transformers for language understanding,” in *Proceedings of the 2019 Conference of the North American Chapter of the Association for Computational Linguistics: Human Language Technologies, Volume 1 (Long and Short Papers)*, J. Burstein, C. Doran, and T. Solorio, Eds. Minneapolis, Minnesota: Association for Computational Linguistics, Jun. 2019, pp. 4171–4186. [Online]. Available: <https://aclanthology.org/N19-1423/>
- [14] A. Botach, E. Zheltonozhskii, and C. Baskin, “End-to-end referring video object segmentation with multimodal transformers,” in *Proceedings of the IEEE/CVF Conference on Computer Vision and Pattern Recognition (CVPR)*, June 2022, pp. 4985–4995.
- [15] J. Wu, Y. Jiang, P. Sun, Z. Yuan, and P. Luo, “Language as queries for referring video object segmentation,” in *Proceedings of the IEEE/CVF Conference on Computer Vision and Pattern Recognition (CVPR)*, June 2022, pp. 4974–4984.
- [16] D. Wu, T. Wang, Y. Zhang, X. Zhang, and J. Shen, “Onlinerefer: A simple online baseline for referring video object segmentation,” in *Proceedings of the IEEE/CVF International Conference on Computer Vision (ICCV)*, October 2023, pp. 2761–2770.
- [17] H. Ding, C. Liu, S. He, X. Jiang, and C. C. Loy, “Mevis: A large-scale benchmark for video segmentation with motion expressions,” in *Proceedings of the IEEE/CVF International Conference on Computer Vision (ICCV)*, October 2023, pp. 2694–2703.
- [18] L. Wen, D. Du, Z. Cai, Z. Lei, M.-C. Chang, H. Qi, J. Lim, M.-H. Yang, and S. Lyu, “Uadetrac: A new benchmark and protocol for multi-object detection and tracking,” *Computer Vision and Image Understanding*, vol. 193, p. 102907, 2020. [Online]. Available: <https://www.sciencedirect.com/science/article/pii/S1077314220300035>
- [19] H. Zhao, X. Wang, D. Wang, H. Lu, and X. Ruan, “Transformer vision-language tracking via proxy token guided cross-modal fusion,” *Pattern Recognition Letters*, vol. 168, pp. 10–16, 2023. [Online]. Available: <https://www.sciencedirect.com/science/article/pii/S0167865523000545>
- [20] L. Zhou, Z. Zhou, K. Mao, and Z. He, “Joint visual grounding and tracking with natural language specification,” in *Proceedings of the IEEE/CVF Conference on Computer Vision and Pattern Recognition (CVPR)*, June 2023, pp. 23 151–23 160.
- [21] Y. Zheng, B. Zhong, Q. Liang, G. Li, R. Ji, and X. Li,

- “Toward unified token learning for vision-language tracking,” *IEEE Transactions on Circuits and Systems for Video Technology*, vol. 34, no. 4, pp. 2125–2135, 2024.
- [22] B. Kang, X. Chen, S. Lai, Y. Liu, Y. Liu, and D. Wang, “Exploring enhanced contextual information for video-level object tracking,” in *AAAI*, 2025.
- [23] H. Zhang, J. Wang, J. Zhang, T. Zhang, and B. Zhong, “One-stream vision-language memory network for object tracking,” *IEEE Transactions on Multimedia*, vol. 26, pp. 1720–1730, 2024.
- [24] T. Brown, B. Mann, N. Ryder, M. Subbiah, J. D. Kaplan, P. Dhariwal, A. Neelakantan, P. Shyam, G. Sastry, A. Askell, S. Agarwal, A. Herbert-Voss, G. Krueger, T. Henighan, R. Child, A. Ramesh, D. Ziegler, J. Wu, C. Winter, C. Hesse, M. Chen, E. Sigler, M. Litwin, S. Gray, B. Chess, J. Clark, C. Berner, S. McCandlish, A. Radford, I. Sutskever, and D. Amodei, “Language models are few-shot learners,” in *Advances in Neural Information Processing Systems*, H. Larochelle, M. Ranzato, R. Hadsell, M. Balcan, and H. Lin, Eds., vol. 33. Curran Associates, Inc., 2020, pp. 1877–1901. [Online]. Available: [https://proceedings.neurips.cc/paper\\_files/paper/2020/file/1457c0d6bfc4967418bfb8ac142f64a-Paper.pdf](https://proceedings.neurips.cc/paper_files/paper/2020/file/1457c0d6bfc4967418bfb8ac142f64a-Paper.pdf)
- [25] J. Ansel, E. Yang, H. He, N. Gimelshein, A. Jain, M. Voznesensky, B. Bao, P. Bell, D. Berard, E. Burovski, G. Chauhan, A. Chourdia, W. Constable, A. Desmaison, Z. DeVito, E. Ellison, W. Feng, J. Gong, M. Gschwind, B. Hirsh, S. Huang, K. Kalambarkar, L. Kirsch, M. Lazos, M. Lezcano, Y. Liang, J. Liang, Y. Lu, C. Luk, B. Maher, Y. Pan, C. Puhersch, M. Reso, M. Saroufim, M. Y. Siraichi, H. Suk, M. Suo, P. Tillet, E. Wang, X. Wang, W. Wen, S. Zhang, X. Zhao, K. Zhou, R. Zou, A. Mathews, G. Chanan, P. Wu, and S. Chintala, “PyTorch 2: Faster Machine Learning Through Dynamic Python Bytecode Transformation and Graph Compilation,” in *29th ACM International Conference on Architectural Support for Programming Languages and Operating Systems, Volume 2 (ASPLOS ’24)*. ACM, Apr. 2024. [Online]. Available: <https://pytorch.org/assets/pytorch2-2.pdf>
- [26] T.-Y. Lin, P. Goyal, R. Girshick, K. He, and P. Dollar, “Focal loss for dense object detection,” in *Proceedings of the IEEE International Conference on Computer Vision (ICCV)*, Oct 2017.
- [27] H. Touvron, T. Lavril, G. Izacard, X. Martinet, M.-A. Lachaux, T. Lacroix, B. Rozière, N. Goyal, E. Hambro, F. Azhar *et al.*, “Llama: Open and efficient foundation language models,” *arXiv preprint arXiv:2302.13971*, 2023.
- [28] J. Lin, J. Chen, K. Peng, X. He, Z. Li, R. Stiefelhagen, and K. Yang, “Echotrack: Auditory referring multi-object tracking for autonomous driving,” *IEEE Transactions on Intelligent Transportation Systems*, vol. 25, no. 11, pp. 18964–18977, 2024.
- [29] W. He, Y. Jian, Y. Lu, and H. Wang, “Visual-linguistic representation learning with deep cross-modality fusion for referring multi-object tracking,” in *ICASSP 2024 - 2024 IEEE International Conference on Acoustics, Speech and Signal Processing (ICASSP)*, 2024, pp. 6310–6314.
- [30] Y. Zhang, C. Wang, X. Wang, W. Zeng, and W. Liu, “Fairmot: On the fairness of detection and re-identification in multiple object tracking,” *International journal of computer vision*, vol. 129, pp. 3069–3087, 2021.
- [31] N. Wojke, A. Bewley, and D. Paulus, “Simple online and realtime tracking with a deep association metric,” in *2017 IEEE International Conference on Image Processing (ICIP)*, 2017, pp. 3645–3649.
- [32] Y. Zhang, P. Sun, Y. Jiang, D. Yu, F. Weng, Z. Yuan, P. Luo, W. Liu, and X. Wang, “Bytetrack: Multi-object tracking by associating every detection box,” in *Computer Vision – ECCV 2022*, S. Avidan, G. Brostow, M. Cissé, G. M. Farinella, and T. Hassner, Eds. Cham: Springer Nature Switzerland, 2022, pp. 1–21.
- [33] C. Liang, Z. Zhang, X. Zhou, B. Li, S. Zhu, and W. Hu, “Rethinking the competition between detection and reid in multiobject tracking,” *IEEE Transactions on Image Processing*, vol. 31, pp. 3182–3196, 2022.
- [34] T. Meinhardt, A. Kirillov, L. Leal-Taixé, and C. Feichtenhofer, “Trackformer: Multi-object tracking with transformers,” in *Proceedings of the IEEE/CVF Conference on Computer Vision and Pattern Recognition (CVPR)*, June 2022, pp. 8844–8854.
- [35] B. Heo, S. Park, D. Han, and S. Yun, “Rotary position embedding for vision transformer,” in *European Conference on Computer Vision (ECCV)*, 2024.
- [36] K. He, X. Zhang, S. Ren, and J. Sun, “Deep residual learning for image recognition,” in *Proceedings of the IEEE Conference on Computer Vision and Pattern Recognition (CVPR)*, June 2016.
- [37] Y. Liu, M. Ott, N. Goyal, J. Du, M. Joshi, D. Chen, O. Levy, M. Lewis, L. Zettlemoyer, and V. Stoyanov, “Roberta: A robustly optimized bert pretraining approach,” 2019. [Online]. Available: <https://arxiv.org/abs/1907.11692>
- [38] J. Luiten, A. Osep, P. Dendorfer, P. Torr, A. Geiger, L. Leal-Taixé, and B. Leibe, “Hota: A higher order metric for evaluating multi-object tracking,” *International journal of computer vision*, vol. 129, pp. 548–578, 2021.
- [39] H. Touvron, M. Cord, M. Douze, F. Massa, A. Sablayrolles, and H. Jegou, “Training data-efficient image transformers & distillation through attention,” in *Proceedings of the 38th International Conference on Machine Learning*, ser. Proceedings of Machine Learning Research, M. Meila and T. Zhang, Eds., vol. 139. PMLR, 18–24 Jul 2021, pp. 10347–10357. [Online]. Available: <https://proceedings.mlr.press/v139/touvron21a.html>
- [40] A. Dosovitskiy, L. Beyer, A. Kolesnikov, D. Weissenborn, X. Zhai, T. Unterthiner, M. Dehghani, M. Minderer, G. Heigold, S. Gelly, J. Uszkoreit, and N. Houlsby, “An image is worth 16x16 words: Transformers for image recognition at scale,” 2021. [Online]. Available: <https://arxiv.org/abs/2010.11929>

- [41] Z. Liu, H. Hu, Y. Lin, Z. Yao, Z. Xie, Y. Wei, J. Ning, Y. Cao, Z. Zhang, L. Dong, F. Wei, and B. Guo, “Swin transformer v2: Scaling up capacity and resolution,” in *Proceedings of the IEEE/CVF Conference on Computer Vision and Pattern Recognition (CVPR)*, June 2022, pp. 12 009–12 019.
- [42] J. Deng, W. Dong, R. Socher, L.-J. Li, K. Li, and L. Fei-Fei, “Imagenet: A large-scale hierarchical image database,” in *2009 IEEE Conference on Computer Vision and Pattern Recognition*, 2009, pp. 248–255.
- [43] A. Geiger, P. Lenz, and R. Urtasun, “Are we ready for autonomous driving? the kitti vision benchmark suite,” in *2012 IEEE Conference on Computer Vision and Pattern Recognition*, 2012, pp. 3354–3361.
- [44] I. Loshchilov and F. Hutter, “Decoupled weight decay regularization,” 2019. [Online]. Available: <https://arxiv.org/abs/1711.05101>
- [45] X. Zhu, W. Su, L. Lu, B. Li, X. Wang, and J. Dai, “Deformable detr: Deformable transformers for end-to-end object detection,” 2021. [Online]. Available: <https://arxiv.org/abs/2010.04159>
- [46] J. Cao, J. Pang, X. Weng, R. Khirodkar, and K. Kitani, “Observation-centric sort: Rethinking sort for robust multi-object tracking,” in *Proceedings of the IEEE/CVF Conference on Computer Vision and Pattern Recognition (CVPR)*, June 2023, pp. 9686–9696.
- [47] Y. Du, Z. Zhao, Y. Song, Y. Zhao, F. Su, T. Gong, and H. Meng, “Strongsort: Make deepsort great again,” *IEEE Transactions on Multimedia*, vol. 25, pp. 8725–8737, 2023.